Journal of Materials Chemistry A

PAPER

View Article Online
View Journal | View Issue

Cite this: J. Mater. Chem. A, 2016, 4, 5654

Experimental and theoretical studies on competitive adsorption of aromatic compounds on reduced graphene oxides†

Shujun Yu,[ab] Xiangxue Wang,[ab] Yuejie Ai,*[a] Xiaoli Tan,[bc] Tasawar Hayat,[de] Wenping Hu*[f] and Xiangke Wang*[ace]

Received 29th January 2016
Accepted 11th March 2016

DOI: 10.1039/c6ta00890a

www.rsc.org/MaterialsA

The individual and competitive adsorption studies of benzene, aniline and naphthylamine on reduced graphene oxides (rGOs) were investigated by batch experiments and theoretical density functional theory (DFT). Experimental results indicate that (1) in all the single, binary, and ternary aromatic compound systems, the sequence of maximum adsorption capacity is naphthylamine > aniline > benzene on rGOs; (2) the overall adsorption capacity of rGOs is in the order of ternary > binary > single system. The DFT calculations indicate that (1) the adsorption energy (E_{ad}) follows the order of E_{ad} (benzene) < E_{ad} (aniline) < E_{ad} (naphthylamine); (2) the binding energy (E_{bd}) values of aromatic mixtures indicate that the intramolecular interactions between the aromatic compounds themselves have an important influence on their adsorption on rGOs. The DFT calculations are in good agreement with the batch adsorption results. These findings are very important and useful to understand the mechanisms of adsorption of aromatic compounds on rGOs as well as assessing the effect of the benzene-ring number and polar functional groups on the adsorption of coexisting aromatic compounds on rGOs. The contents are important for the application of rGOs in environmental pollution management.

Introduction

Aromatic compounds are the second most abundant family of organic constituents present in the biosphere after carbohydrates. Aromatic pollutants are widely found in the effluents from the pharmaceutical, petrochemical, dyestuff, pesticide, and other industries.[1] It is also well-known that such organic pollutants are highly toxic, mutagenic and/or carcinogenic to natural microflora as well as to higher systems including humans.[2] The efficient elimination of the persistent aromatic pollutants from aqueous solutions has been studied extensively by photocatalysis, electrolysis, adsorption, biodegradation and membrane filtration.[3–7] Among these methods, the adsorption technique has been used widely due to its low cost, easy operation and practical applications in large scale.[8–12] Clay-based materials have been studied intensively for the removal of aromatic pollutants from aqueous systems.[8–10] Jiang *et al.* reported that the removal capacity of aniline for manganese oxide modified diatomite was 42.9 mg g^{-1}.[9] Due to stronger hydrophobicity of 2-naphthol and its structural properties, the adsorption amount of 2-naphthol on organo-montmorillonite is as nearly five times as that of phenol.[8] Radian and Mishael have demonstrated the enhanced adsorption of pyrene to polycation–montmorillonite composites in the presence of humic acid, attributed to strong electrostatic interactions.[10] However, the low adsorption capacities or efficiencies of these materials have obviously restricted their applications.

Due to its large surface area and unique structure, potential environmental applications of graphene-based materials as superior adsorbents have been suggested for the removal of toxic chemicals from the natural environment.[13–16] However, with the widespread use of graphene-based materials, it is inevitable that graphene may be released into the environment as a contaminant during production, transport and disposal processes. The toxicity of graphene-based materials to various types of organisms (*e.g.*, bacteria, algae, plants, invertebrates, and fish) has been demonstrated in recent studies.[17–19] Zhao *et al.*[20] concluded that graphene-based materials are more toxic

[a]School of Environment and Chemical Engineering, North China Electric Power University, Beijing 102206, P. R. China. E-mail: xkwang@ncepu.edu.cn; aiyuejie314@126.com

[b]Key Laboratory of Novel Thin Film Solar Cells, Institute of Plasma Physics, Chinese Academy of Sciences, Hefei 230031, P. R. China

[c]Collaborative Innovation Center of Radiation Medicine of Jiangsu Higher Education Institutions, School for Radiological and Interdisciplinary Sciences, Soochow University, Suzhou 215123, P.R. China

[d]Department of Mathematics, Quaid-I-Azam University, Islamabad 44000, Pakistan

[e]NAAM Research Group, Faculty of Science, King Abdulaziz University, Jeddah 21589, Saudi Arabia

[f]Key Laboratory of Organic Solids, Institute of Chemistry, Chinese Academy of Sciences, Beijing 100190, P. R. China. E-mail: huwp@iccas.ac.cn; Fax: +86-1061772890; Tel: +86-1061772890

† Electronic supplementary information (ESI) available: Additional preparation and characterization of rGOs. More detailed information on DFT calculations, and the parameters of model simulation. See DOI: 10.1039/c6ta00890a

than conventional carbon materials such as black carbon and graphite. Coexistence of graphene-based materials with pollutants in aquatic environments could alter the transport, accumulation and toxicity of both constituents.[20] Therefore, knowledge of the adsorption behavior of toxic chemicals by graphene-based materials is critical for the application of graphene-based materials and environmental risk assessment of both graphene-based materials and toxic chemicals.

Graphene oxide (GO) is a graphene sheet with carboxylic groups at its edges and phenolic hydroxyl and epoxide groups on its basal plane. Thermal annealing or chemical treatment can eliminate functional groups on GO to produce reduced graphene oxide (rGO).[18] In contrast to GO, rGO is a better adsorbent for aromatic pollutants due to its higher hydrophobicity, higher surface area and lower oxygen content. Chen *et al.*[12] studied the adsorption of *m*-dinitrobenzene, nitrobenzene, and *p*-nitrotoluene onto GO, rGO and graphene nanosheets. They found that rGO nanosheets, which had more defect sites than GO or graphene nanosheets, resulted in the highest adsorption of nitroaromatic compounds which was 10–50 times greater than the reported adsorption of carbon nanotubes (CNTs). While, compared with CNTs, studies regarding the interactions of rGO with organic pollutants have only recently begun, and only single-solute adsorption was examined. However, multiple organic contaminants are often simultaneously present in a natural aqueous solution. While single-solute adsorption studies may adequately predict the retention of strongly bonded species, adsorption of less strongly bonded species is more likely to be affected by the presence of competing species in systems with multiple organic contaminants. Competitive adsorption and displacement of multiple organic contaminants on rGO would likely be observed in multi-solute systems, as observed on CNTs, activated carbon and natural geosorbents.[21–23] Assessments of potential bioavailability and toxicity of organics in contaminated solutions may depend on whether experiments are performed using single- or multi-organic solutions. Therefore, it is valuable to understand the alteration caused by competitive adsorption and the underlying mechanisms.

Aromatic compounds such as benzene and toluene are organic compounds that are classified as flammable, toxic, carcinogenic, and/or mutagenic agents. These compounds, however, are often employed in chemical processes as raw materials or even as solvents.[24] In the United States, gasoline is generally composed of 2% benzene by volume but the concentration of benzene in gasoline may be up to 5% in other countries.[25] It should be noted that benzene, with a water solubility of 1750 mg L^{-1}, is more water soluble than other major gasoline components. The United States Environmental Protection Agency (EPA) and Taiwan EPA have both set the maximum contaminant level for benzene in drinking water and groundwater at 0.005 mg L^{-1}.[25] According to the recent studies, the main adsorption mechanism of benzene is π–π interactions between the π orbital on the carbon basal planes and the electronic density in the benzene aromatic rings.[25] Generally, π–π interactions depend on the size and shape of the aromatic system and the substitution unit.[26] An increasing number of theoretical (calculation or simulation) studies indicated that the π–π interactions between aromatic adsorbates and CNTs increased with increasing aromatic rings in adsorbate molecules; both electron-withdrawing (*e.g.*, $-NO_2$ and –Cl) and electron-donating (*e.g.*, $-NH_2$ and –OH) substituents on benzene could enhance the adsorption to CNTs.[26,27] Similarly, Chen *et al.*[12] used spectroscopy to evidence that the strong adsorptive interactions of nitroaromatic compounds onto rGO resulted from π–π interactions between the nitroaromatic molecules (electron acceptors) and graphene nanosheets (electron donors) of rGO. However, no studies have investigated the molecular-level mechanisms of aromatic amine compound adsorption onto rGO. In addition, spectroscopic evidence is required to prove the occurrence of site-specific π–π interactions or charge transfer processes.

Aniline and naphthylamine are selected as the representative of the aromatic amine compounds because they are widely used as intermediates in the synthesis of dyes and other chemicals and are common organic pollutants. The main objectives of the present study were (1) to investigate the individual and competitive adsorption of benzene (labeled as Ben), aniline (BN) and naphthylamine (NA) on rGOs from aqueous solutions; (2) to demonstrate the different interaction mechanisms of Ben, BN and NA on rGOs by using spectroscopic techniques and theoretical calculations; (3) to compare the adsorption processes of Ben, BN and NA onto rGOs and observe the specific electron transfer between the aromatic compounds and rGOs by spectroscopic methods (FTIR and Raman); (4) to discuss the interaction mechanism of the aromatic compounds with rGOs by using density functional theory (DFT) calculations. The results would help to understand the effect of the benzene-ring number and polar functional groups on the adsorption of coexisting aromatic compounds on graphene-based materials.

Experimental

Materials

The rGOs were prepared by reducing graphene oxides (GOs) according to the previously reported method.[28] More detailed procedures on the synthesis of GOs and rGOs are provided in the ESI.† Graphite flake (48 μm, 99.95% purity) was purchased from Qingdao Tianhe graphite Co., Ltd. Benzene (≥99.9% purity), aniline (≥99.5% purity) and naphthylamine (≥99.0% purity) were obtained from Sigma-Aldrich. Benzene, aniline and naphthylamine stock solutions (300 mg L^{-1}) were prepared by dissolving them in absolute ethyl alcohol and then were diluted using Milli-Q water. All other chemicals of analytical reagents were purchased from Sinopharm Chemical Reagent Co., Ltd.

Characterization

The rGOs before and after adsorption of aromatic compounds were characterized by using Fourier-transform infrared spectroscopy (FTIR) and Raman spectroscopy. The FTIR spectrum was recorded by a Bruker Tensor 27 FTIR spectrophotometer in the range of 4000–400 cm^{-1} using the KBr disc technique. Raman spectroscopy was carried out on the InVia Reflex Raman

spectrometer (Renishaw) at 532 nm. More detailed characterizations of the prepared rGOs using techniques such as transmission electron microscopy (TEM), X-ray photoelectron spectroscopy (XPS), electron energy loss spectroscopy (EELS), thermogravimetric analysis (TGA) and potentiometric acid–base titrations are provided in Fig. 1. The TEM image was obtained by a transmission electron microscope (JEM-1011, Japan). The XPS data were acquired with a Thermo Escalab 250 XPS using Al Kα radiation at 150 W. EELS analyses were carried out using an ultra-high vacuum (base pressure of chamber $< 1 \times 10^{-7}$ Pa) JEM-2000VF scanning transmission electron microscope (STEM) operated at 200 kV with a field emission electron gun. TGA measurements were taken by using a Shimadzu TGA-50 thermogravimetric analyzer from room temperature to 973 K at a heating rate of 10 K min^{-1} with a nitrogen rate of 50 mL min^{-1}. Potentiometric titrations were conducted by using a computer-controlled titration system (DL50 Automatic Titrator, Mettler Toledo).

Batch adsorption experiments

The effect of pH on the adsorption of Ben, BN and NA onto rGOs was investigated by using the batch technique in 8 mL brown glass vials equipped with polytetrafluoroethylene-lined screw caps at 0.1 g L^{-1} of adsorbent concentration (m/V) at 298 K. The pH of the suspension was adjusted with 0.01–1.0 mol L^{-1} $HClO_4$ or NaOH solution on a digital pH meter (PHS-3C). Before and after sorption, variances in pH were kept below 0.1. For the adsorption isotherm of single aromatic compounds, stock suspensions of rGOs, $NaClO_4$, and aromatic compounds were added into the glass vials, and the difference in the total volume of the mixtures was compensated by Milli-Q water to achieve the desired concentrations of different components. The competitive adsorption of aromatic compounds in binary and ternary systems of Ben/BN, Ben/NA, BN/NA and Ben/BN/NA on rGOs was investigated by using the same initial molar concentration of each aromatic compound. After the glass vials were oscillated for 48 h to ensure the adsorption equilibrium, the solid and liquid phases were separated by centrifugation at 5595g for 30 min. The blank experiments (without rGOs) were included in each set of adsorption experiments to eliminate the mass loss during the experimental processes. The concentrations of Ben, BN and NA were analyzed by ultraviolet-visible (UV-vis) spectroscopy at the wavelengths of 205, 280 and 236 nm, respectively. More details on the measurement of Ben, BN and NA are provided in the ESI.† Each experimental dataset was obtained by the average values of triple parallel samples (the resulting error bars (within ±5%) are provided).

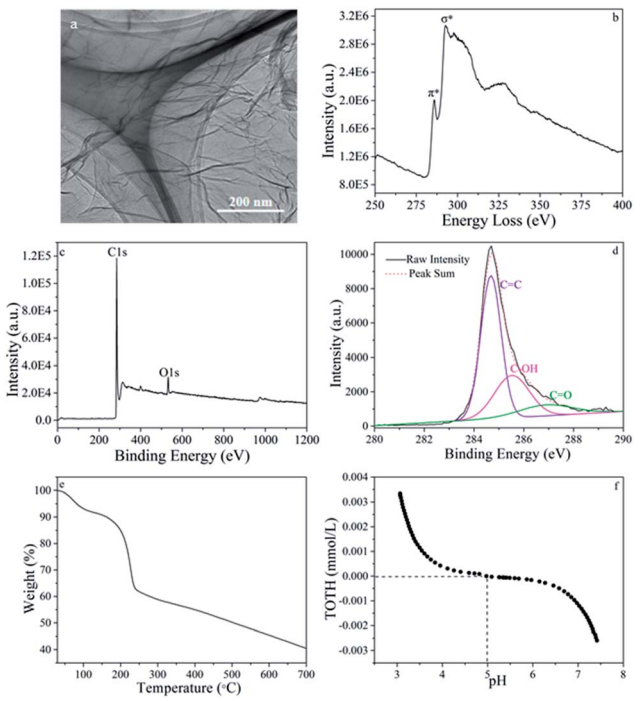

Fig. 1 The characterization of rGOs: (a) TEM image; (b) EELS spectrum; (c) XPS survey spectrum; (d) C 1s spectrum; (e) TGA analysis; (f) potentiometric acid–base titrations.

Computational details

The interaction mechanism of aromatic compounds with rGOs/GOs was demonstrated by using the B3LYP hybrid functional of density functional theory (DFT) with the 6-31G (d) basis set.[29–31] The dispersion forces and solvation effects were corrected by the empirical formula of Grimme[32–34] and a conductor-like polarizable continuum model (CPCM),[35–37] respectively. The nature of local minima was confirmed by analytical calculations of the Hessian by frequency calculations performed at the same level of theory as in the optimizations. All calculations were carried out with the Gaussian 09 software package.[38]

The optimized geometries of Ben, BN and NA are shown in Fig. S1.† The rGOs may have some remaining oxygen-containing functional groups because of the incomplete reduction, so three finite-sized molecular models of rGOs and GOs were employed in DFT calculations (Fig. S2†). The adsorption energy (E_{ad}) was calculated as: $E_{ad} = E_G + E_x - E_{G-x}$, where E_G, E_x and E_{G-x} correspond to the total energies of the adsorbents (rGOs or GOs), aromatic compounds (Ben, BN and NA) and the combined system, respectively. A positive value of the E_{ad} indicates that the adsorption is exothermic and the graphene composite system is stable.

Results and discussion

Characterization

TEM acts as "our eyes" enabling us not only to reveal the morphology, but also to provide structural, chemical and electronic information of rGOs at the atomic level.[39,40] In Fig. 1a, the rGOs present a large, entangled and almost transparent morphology. The nearly invisible areas are due to the ultrathin nature of graphene nanosheets, while the relative clear ones are the multilayered stacks of the graphene sheets.[39] The electronic structure of the rGOs was confirmed by EELS (Fig. 1b), with its spectrum exhibiting the characteristic graphitic 1s–π* and 1s–σ* peaks in the K-edge region at 285.86 and 292.61 eV, respectively.[40]

No peak for oxygen K-edge (532 eV) was observed in the spectra, indicative of minimal oxygen groups in the material.

FTIR and XPS are very powerful techniques that are commonly used to elucidate the electronic structures and elemental compositions, including the oxidation state of an element in the given material.[41] In Fig. 1d, the XPS spectrum of rGOs shows a dominant peak of sp^2 C=C at 284.7 eV, which is attributed to the graphitic structure. Several small peaks of C–OH at 285.5 eV and C=O at 286.9 eV are assigned to carbon atoms attached to different oxygen-containing moieties.[12] Furthermore, the ratio of C=C/C–OH/C=O calculated from the ratio of C=C/C–OH/C=O XPS peak area was 5 : 2.5 : 1. The atomic ratio of carbon to oxygen calculated from the XPS survey spectrum (Fig. 1c) was 5.5. As illustrated in Fig. 4a, the FTIR spectrum of rGOs shows characteristic bands at 1053 and 1121 cm^{-1} (C–O bond),[42] at 1439 cm^{-1} (stretching of benzene ring),[43] at 1576 and 1632 cm^{-1} (sp^2 C–C bond)[44] and at 3433 cm^{-1} (OH stretching vibration).[42]

Raman spectroscopy was over long periods of time accepted as an important tool in the characterization of rGOs. The main features in the Raman spectrum of carbons are the so-called "G" and "D" peaks, which lie at around 1580 and 1350 cm^{-1} respectively for visible excitation (Fig. 4b).[45] The "G" peak is assigned to the bond stretching modes for all pairs of sp^2 atoms in both rings and chains. The "D" peak is from the breathing modes of sp^2 atoms in the rings. The I_D/I_G ratio is used to estimate the relative extent of structural defects.[46] The value of I_D/I_G of rGOs (0.943) is higher than that of GOs (0.926),[16] revealing a decrease in the average size of the sp^2 domains after the reduction of GOs.[28]

TGA is a complementary technique that can reveal the composition and changes in thermal stability of the samples.[47] The curve of rGOs exhibits two mass losses around 100 and 200 °C (Fig. 1e). Although it starts to lose mass upon heating even below 100 °C, the major mass loss occurs at ~200 °C, presumably due to pyrolysis of the labile oxygen-containing functional groups, yielding CO, CO_2, and steam.[42]

The acid–base surface properties of rGOs are investigated by acid–base titration and the fitting curve is displayed in Fig. 1f. The pH of zero point charge (pH_{ZPC}) of rGOs is about 5.0, which indicates that the surface of rGOs is positively charged at pH < 5.0 and negatively charged at pH > 5.0.

Adsorption isotherms

The adsorption isotherms of the three single aromatic compounds on rGOs are displayed in Fig. S3.† The data are simulated by the widely used Langmuir[48] and Freundlich[49] isotherm models to understand the adsorption mechanism. More detailed description and the corresponding parameters of Langmuir and Freundlich models are presented in Table S1.† The criteria for the selection of the isotherm model were the correlation coefficient and maximum deviation based on the predicted values. As evidenced from Table S1 and Fig. S3,† the Langmuir model gives a somewhat better fit than the Freundlich model, implying that monolayer coverage is the main adsorption mechanism. The maximum adsorption capacity of NA on rGOs is higher than those of the other two aromatic compounds, and their maximum adsorption capacities (Q_{max}) are 2.96, 2.75, and 2.27 mmol g^{-1} for NA, BN and Ben, respectively. In addition, Sips isotherm is a combined form of Langmuir and Freundlich expressions deduced for predicting the heterogeneous adsorption systems.[50] The results of Table S1 and Fig. S3† show that the Sips model is very good in predicting the experimental data and further evidence that the adsorption of aromatic compounds is heterogeneous adsorption.

To study the involved interactions during the adsorption process, a single adsorbate is normally chosen. However, pollutants are regularly manifold and complex in wastewaters. Nevertheless, studies of multicomponent systems are less frequent even if they are closely related to improve the efficiency of water treatment. Therefore, the competitive adsorption of aromatic compounds in the mixtures of Ben/BN, Ben/NA, BN/NA and Ben/BN/NA on rGOs was investigated herein by using the same initial amount of each aromatic compound. The adsorption isotherms of Ben, BN and NA with and without competitors onto rGOs are shown in Fig. 2. Langmuir, Freundlich and Sips models were used to fit the adsorption data (Table 1). The Freundlich model had good fits for multi-solute isotherms, but it failed to fit the single-solute isotherms. These results showed that the multi-solute adsorption onto rGOs is multilayer heterogeneous adsorption.

Compared to a single aromatic compound system, the Q_{max} values of the three aromatic compounds decreased in both binary and ternary systems. For example, the Q_{max} of BN in the single system was decreased from 2.75 to 2.14, 1.29 and 0.91 mmol g^{-1} in Ben/BN, BN/NA and Ben/BN/NA systems, respectively (shown in Fig. 2b). A similar phenomenon was also observed for Ben and NA. The results indicate that there is

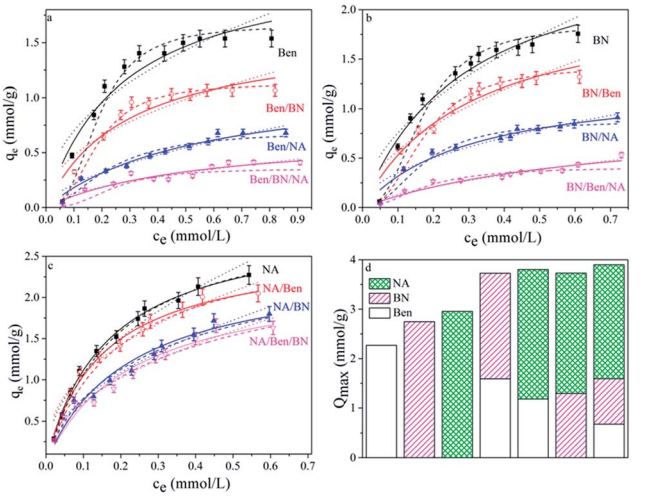

Fig. 2 Adsorption isotherms of Ben (a), BN (b) and NA (c) in a single system, binary systems (Ben/BN, Ben/NA, BN/NA) and a ternary system (Ben/BN/NA) on rGOs at pH = 6.5 ± 0.1, I = 0.01 mol L^{-1} $NaClO_4$, m/V = 0.1 g L^{-1}, T = 298 K. The solid lines represent the Langmuir model. The dotted lines represent the Freundlich model. The dashed lines represent the Sips model. (d) Maximum adsorption capacities of aromatic compounds adsorbed on rGOs in single, binary and ternary systems.

Table 1 Results of Langmuir, Freundlich and Sips models fit to adsorption data of Ben, BN and NA on rGOs

		Langmuir model			Freundlich model			Sips model		
Aromatic compounds	With competitors	q_{max} (mmol g^{-1})	b (L $mmol^{-1}$)	R^2	K_F ($mmol^{1-n}$ L^n g^{-1})	n	R^2	K_s (L g^{-1})	n_s	R^2
Ben	None	2.267	3.665	0.902	2.004	0.489	0.802	152.801	2.718	0.943
	BN	1.591	3.485	0.902	1.350	0.454	0.979	92.539	2.584	0.976
	NA	1.183	1.805	0.967	0.817	0.584	0.990	11.371	1.865	0.973
	BN/NA	0.678	1.853	0.882	0.468	0.567	0.989	15.751	2.670	0.916
BN	None	2.746	3.405	0.939	2.592	0.558	0.875	153.650	2.497	0.960
	Ben	2.138	3.302	0.933	1.928	0.524	0.986	108.350	2.469	0.966
	NA	1.293	3.248	0.956	1.115	0.497	0.983	43.728	2.207	0.978
	Ben/NA	0.913	1.477	0.924	0.603	0.658	0.994	15.262	2.058	0.970
NA	None	2.956	6.050	0.995	3.275	0.482	0.962	18.024	1.037	0.994
	Ben	2.618	6.677	0.991	2.760	0.412	0.970	14.492	0.998	0.982
	BN	2.437	4.439	0.962	2.444	0.503	0.979	6.761	0.808	0.972
	Ben/BN	2.307	4.287	0.949	2.233	0.487	0.980	5.350	0.758	0.963

competition among the aromatic compounds for adsorption on rGOs. The extent of the decrease is expected to relate to the adsorption affinity of rGOs to the coexisting aromatic compounds. NA lowers BN and Ben adsorption significantly instead of *vice versa*, and BN lowers Ben adsorption instead of *vice versa*, thus indicating the order of the adsorption affinity to be NA > BN > Ben, which is in good agreement with the results of the single system. As compared with the molecular structure of aromatic compounds, functional groups of BN/NA (*i.e.*, $-NH_2$ group) should be responsible for the decreased Ben adsorption because these groups can form hydrogen-bonding with oxygen-containing functional groups in rGOs. Adsorption capacity of BN decreases significantly with NA as the competitor (Fig. 2b). The strength of π–π stacking and hydrogen-bonding interactions depend on the solute π-polarity ability (π*) and hydrogen-bonding acceptor ability (β_m), respectively, which are significantly related to the number of aromatic rings.[51] According to the π* and β_m values of aromatic hydrocarbons studied here in the order of benzene (π* = 0.59 and β_m = 0.10) < aniline (π* = 0.73 and β_m = 0.50) < 1-naphthylamine (π* = 0.83 and β_m = 0.50), it is reasonable that NA shows a strong competitive adsorption effect to BN because of its extra benzene-rings.[52]

As can be seen from Fig. 2d, partitioning adsorption of the aromatic compounds on rGOs follows the sequence of NA > BN > Ben in all systems. Even the mutual inhibition is seen for all binary and ternary systems, and the overall adsorption capacity of rGOs is greater than the single systems. This phenomenon shows that the adsorption sites of Ben, BN and NA are likely to be different and intra-molecular interactions among the aromatic compounds themselves have a great influence on their adsorption on rGOs.

Possible mechanisms for adsorption and competition

The adsorption mechanisms of rGOs at the molecular level are highly dependent on the structure of the sorbate as a probe and the adsorptive sites of the rGOs because rGO adsorptive sites include flat π networks, wrinkles, defects, and functional groups attached to the surfaces and edges of the graphene nanosheets.[12] As can be seen in Fig. 2, the adsorption heterogeneity appeared due to the the variations and complexity of adsorptive sites of rGO surfaces. Therefore, different mechanisms may act simultaneously, mainly hydrophobic interactions, π–π bonds, electrostatic interactions, and hydrogen bonds.

Due to their hydrophobic surfaces, hydrophobic interactions between rGOs and aromatic compounds are expected. If hydrophobic interactions are the only mechanism for the interactions between organic chemicals and rGOs, the adsorption can be predicted using the hydrophobic parameters of aromatic compounds, such as K_{OW} (octane–water distribution coefficient). The K_{OW} value of the aromatic compounds was in the order of BN < Ben < NA (Table S2†). BN adsorption was higher than Ben, although Ben is more hydrophobic than BN suggesting that other mechanisms besides hydrophobic interactions also contributed to their adsorption.

To assess the contributions of hydrogen bonding to Ben, BN and NA adsorption, the effects of solution pH on adsorption by rGOs were investigated. The effect of pH on Ben, BN and NA adsorption onto rGOs is shown in Fig. 3. The removal efficiency of Ben remained nearly unchanged as the solution pH was altered; thus, H-bonding mechanisms can be ruled out. Similarly, Chen *et al.* ruled out H-bonding mechanisms in the

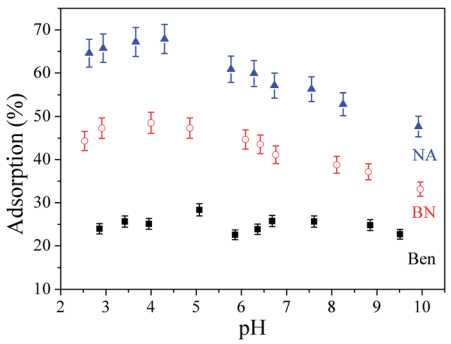

Fig. 3 Effect of pH on Ben, BN and NA adsorption onto rGOs. C_0 = 25 mg L^{-1}, I = 0.01 mol L^{-1} $NaClO_4$, m/V = 0.1 g L^{-1}, T = 298 K.

adsorption of nitroaromatic compounds onto graphene materials because the value of adsorption amount remained constant when the pH changed.[12] The adsorption of BN and NA increases with increasing pH and then the adsorption decreases slightly when pH > pK_a. The unfavourable adsorption of BN/NA at pH > pK_a could be due to the electrostatic repulsion between anionic BN/NA and negatively charged surfaces of rGOs. Besides, with the increase of pH in alkaline solution, the formation of hydrogen bonds is more difficult, and the adsorption capacities decreased. At lower pH values, the higher concentration of H^+ in solution makes more BN and NA molecules protonated. The hydrogen bond (O–H···N hydrogen bond and N–H···O hydrogen bond) between rGOs and BN or NA was weaker, resulting in a lower adsorption capacity. Furthermore, the formation of electrostatic interaction was heavily hampered. As a consequence, the uptake declines sharply.

The π–π electron donor–acceptor interactions (π–π EDA) have been widely used to address the adsorption of organic compounds of sufficient π-acceptor or π-donor strength on the graphene surface.[16] For example, McDermott and McCreery reported that the basal plane of graphite in the vicinity of the edges is often electron-rich, while the regions in the center of the graphene surface are typically electron-depleted.[53] The amino group (–NH_2) is a strong electron-donating group, and the unshared pair of electrons of nitrogen can result in strong electron conjugation with the π electrons in the benzene rings, making the benzene rings electron-rich.[54] Accordingly, the electron-rich benzene rings can interact strongly with polarized positively charged regions on rGOs *via* π–π EDA interaction, causing extremely strong adsorption of BN and NA. Several literature studies are consistent with the proposed mechanism. Chen *et al.* reported that π–π EDA interaction resulted in stronger adsorption of hydroxyl- and amino-substituted aromatics than nonpolar aromatics on carbon nanotubes.[55] Chen and his colleagues found more defect sites in rGO than GO and graphene, resulting in the highest nitroaromatic adsorption.[12] It is necessary to note that, even though both BN and NA contain the –NH_2 group, the adsorption-enhancement effect of the EDA interactions was more prominent for NA. This remarkable difference may be associated with the molecular size and geometry difference between the molecules. NA is a two-ring molecular species with a large π-electron system, which makes it more suitable for adsorption by π–π EDA interaction than the single-ringed BN. The π–π EDA interaction between the rGOs and these aromatic compounds was confirmed using FTIR and Raman spectra. As illustrated in Fig. 4a, the FTIR spectra of rGOs show characteristic bands at 1576 and 1632 cm^{-1} (sp^2 C–C bond)[44] and at 3433 cm^{-1} (OH stretching vibration).[42] Small shifts in the sp^2 C–C bond (1500–1700 cm^{-1}) region were observed after adsorption. These shifts may be due to π–π interactions between the benzene ring of the aromatic compound and the electron-depleted area of the rGOs. The stretching vibrational frequencies of the O–H bond changed after the adsorption, from 3433 to 3429 cm^{-1} for Ben, from 3433 to 3427 cm^{-1} for BN and from 3433 to 3421 cm^{-1} for NA, respectively. This further indicates that π–π interactions exist in the aromatic-rGO systems. Similarly, Zou *et al.* reported

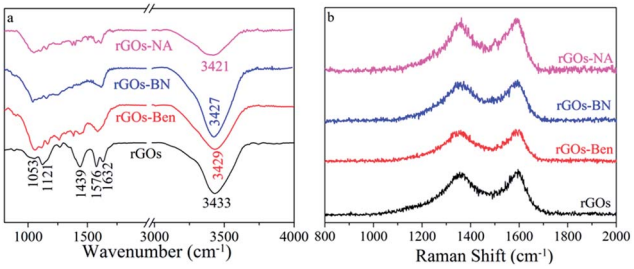

Fig. 4 The characterization of rGOs before and after the adsorption of Ben, BN and NA: (a) FTIR spectra; (b) Raman spectra.

that the O–H bond of the single walled carbon nanotube (SWCNT) changed after the adsorption, from 3846.93 to 3842.85 cm^{-1} for phenol and from 3599.84 to 3543.48 cm^{-1} for aniline, respectively.[56] Raman spectroscopy is usually used to investigate the vibrational properties of carbon structures, and it allows us to determine their crystallization. The peak at ~1582 cm^{-1} (G band) corresponding to the E_{2g} mode of graphite is related to the vibration of sp^2-bonded carbon atoms in a 2-dimensional hexagonal lattice, while the peak at ~1352 cm^{-1} (D band) is assigned to the defects and disorders in the hexagonal graphitic layers (Fig. 4b).[57] The I_D/I_G ratio is used to estimate the relative extent of structural defects.[58] The value of I_D/I_G of rGOs (0.943) is lower than those of rGOs–Ben (0.964), rGOs–BN (0.971) and rGOs–NA (1.001), revealing a decrease in the average size of the sp^2 domains after the adsorption of aromatic compounds. On the basis of the above analysis, we proposed that π–π EDA interactions and hydrogen bonding were the primary mechanism for the adsorption of BN and NA, while π–π EDA interactions were the primary mechanism for the adsorption of Ben.

The adsorption capacity of aromatics is associated with the size and shape of the aromatic system and the substitution unit. Both Ben and BN have one benzene ring in their molecular structure, and the only difference in their structure is that BN has an additional amino group. The amino group on BN can interact with O-containing groups at the surfaces of rGOs *via* hydrogen bonding thus enhancing their interaction. BN and NA have similar molecular structure, but compared with BN, NA would be more polarizable due to its larger molecular weight thus having greater dispersive force with highly polarizable graphene sheets of individual rGOs. Therefore, the adsorption capacity of three aromatics on rGOs was in the order NA > BN > Ben. The competitive adsorption behavior occurs if the competing adsorbate is more strongly adsorbed than the target compound, out competing it for the limited number of adsorption sites available at rGOs. Although the single aromatic removal efficiency was decreased, the overall adsorption capacity of rGOs was increased in all binary and ternary systems. In this case, therefore, we assume that the solute-coated adsorbent surface will be available for the adsorption of other solutes. Due to the hydrophilic nature of amino group in the NA structure, its amino group would preferentially be attracted to rGOs' surfaces *via* hydrogen bond interactions while leaving its hydrophobic benzene rings facing the aqueous phase. The outward benzene ring of NA thus may have created

new adsorption sites, so a second layer of NA or BN or Ben would be sorbed to the initially sorbed NA molecules through π–π and hydrophobic interactions between benzene rings. Significant adsorption of BN by NA particles (Fig. S4†) means molecule–molecule attraction between different solutes, consistent with our assumption. The same mechanism was employed to interpret the cooperative adsorption of aromatic compounds on the multiwalled carbon nanotube (MWCNT).[21,59]

DFT calculation

Considering the complexity of the actual environment, the interaction mechanism of Ben, BN and NA with rGOs/GOs was further demonstrated by using DFT calculations. The most stable optimized structures of three aromatic compounds on rGOs and GOs are shown in Fig. 5 and Fig. 6, respectively, and their corresponding adsorption energies (E_{ad}) are summarized in Table 2.

As shown in Fig. 5, the three aromatic compounds lie parallel to the basal plane of rGOs. The distance between the aromatic ring and the plane of rGOs is around 3.3 Å. The adsorption energies of E_{ad} for Ben, BN and NA are 11.55, 14.45, and 21.01 kcal mol^{-1}, respectively, which are consistent with the experimental maximum adsorption capacity of rGOs for Ben, BN and NA. As presented in former studies, the π–π EDA interaction and hydrogen bonding play an important role in the adsorption of aromatic compounds on rGOs/GOs.[16,60] Compared to the Ben molecule, the BN molecule possesses a polar amino group which may form hydrogen bond with the functional groups on the basal plane. Meanwhile, the NA molecule has an extra aromatic ring and also the amino group. Therefore, in contrast to the Ben molecule, the BN and NA molecules have potentially higher adsorption capacity on the rGOs/GOs. Fig. 6 shows the stable structures of three aromatic compounds with the –O– and –OH groups on the basal plane of GOs. The effect of hydrogen bonding strengthens and the interaction between the aromatic ring and the plane of rGOs with a closer distance of around 3.1–3.2 Å is found. For instance, the NA molecule forms a hydrogen bonding at the bond length of 2.087 Å with the

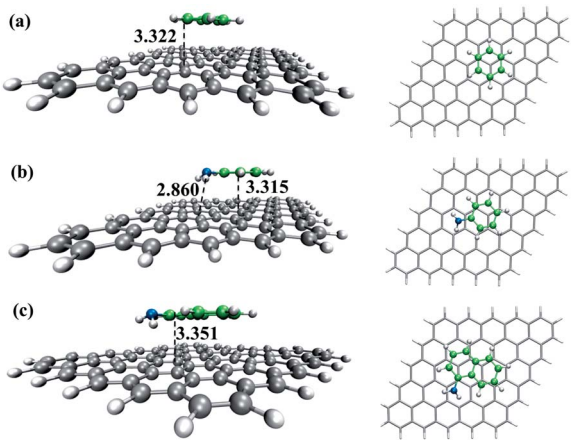

Fig. 5 Side and top view of the optimized geometrical structures for the adsorption of Ben (a), BN (b) and NA (c) on rGOs.

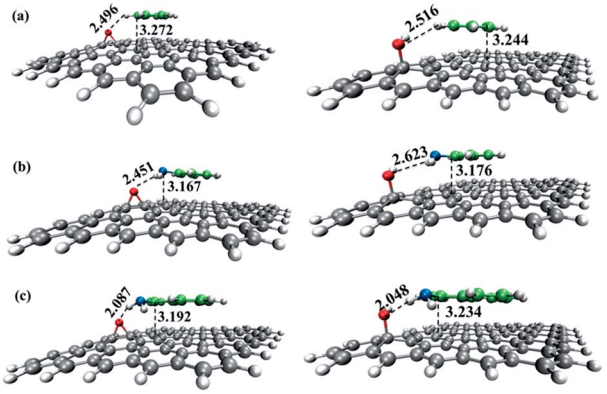

Fig. 6 Optimized geometrical structures for the adsorption of Ben (a), BN (b) and NA (c) on GOs (left: GO(O), right: GO(OH)).

functional –O– group on the basal plane of GOs. This brings stronger overlapping π-clouds of the aromatic rings and adsorbents with the decreased distance of 3.192 Å. As shown in Table 2, the E_{ad} value of "GO(O)–NA" is 27.33 kcal mol^{-1} which is much higher than that of "GO(O)–Ben" (13.30 kcal mol^{-1}) and "GO(O)–BN" (17.96 kcal mol^{-1}). The same conclusion can be found in the GO(OH) models. The E_{ad} values of Ben, BN and NA with –OH group on the basal plane of GOs are calculated to be 14.10, 17.63 and 28.35 kcal mol^{-1}, respectively. Therefore, based on the results of DFT calculations, the adsorption energy follows the order of E_{ad} (Ben) < E_{ad} (BN) < E_{ad} (NA), which is in good agreement with the experimental results.

Interestingly, in aqueous solution, except for the adsorption between the aromatic compounds and the rGOs, there are also intra-molecular interactions between the aromatic compounds themselves. We then optimized the stationary structures and calculated the binding energies for different aromatic dimers. The structures and the binding energies are summarized and presented in Fig. S5† and Table 2, respectively. As shown in Table 2, the calculated binding energies are smaller than the adsorption energies of aromatic rGOs/GOs complexes. Thus, the adsorption mechanism is the dominant process compared to the intra-molecular interactions. As a result, if a stronger adsorption substance is mixed into the single species, the total adsorption

Table 2 Optimized adsorption energies (E_{ad}) of aromatic compounds on rGOs and GOs and optimized binding energies (E_{bd}) ($E_{bd} = E_A + E_B - E_{AB}$) of aromatic mixtures

Systems	E_{ad} (kcal mol^{-1})	Mixtures	E_{bd} (kcal mol^{-1})
rGOs–Ben	11.55	Ben–Ben	3.10
rGOs–BN	14.45	Ben–BN	3.43
rGOs–NA	21.01	Ben–NA	6.30
GO(O)–Ben	13.30	BN–BN	7.64
GO(O)–BN	17.96	BN–NA	7.98
GO(O)–NA	27.33	NA–NA	10.42
GO(OH)–Ben	14.10		
GO(OH)–BN	17.63		
GO(OH)–NA	28.35		

capacity will increase eventually. For instance, the maximum adsorption capacity order of Q_{max} (Ben) < Q_{max} (Ben–BN) < Q_{max} (Ben–NA), Q_{max} (BN) < Q_{max} (BN–NA) is attributed to the single molecule E_{ad} value in the order of E_{ad} (Ben) < E_{ad} (BN) < E_{ad} (NA). On the other hand, when a weaker adsorption substance is mixed into the single phase, the single phase is more like diluted and the strong intra-molecular interactions of the single phase are then weakened. For instance, the E_{bd} of the BN–BN dimer is 7.64 kcal mol^{-1}, indicating that 7.64 kcal mol^{-1} is needed for the free BN molecule to be released from the dimer and then it may adsorb on rGO/GOs. While the E_{bd} of the Ben–BN dimer is only 3.43 kcal mol^{-1} which is much lower than that of the BN–BN dimer, thus there is higher probability for single adsorption resulting in Q_{max} (BN) < Q_{max} (Ben–BN). Similarly, when the single NA molecules are mixed in the "weaker" BN or Ben molecules, its binding energy of the dimer (10.42 kcal mol^{-1}) is diluted by the NA–BN dimer (7.98 kcal mol^{-1}) and NA–Ben dimer (6.30 kcal mol^{-1}). Therefore, more free molecules are attracted to the basal plane of rGOs/GOs and results in Q_{max} (NA) < Q_{max} (NA–BN) < Q_{max} (NA–Ben).

Conclusions

In conclusion, we have investigated the individual and competitive adsorption of benzene, aniline and naphthylamine on rGOs by batch experiments and DFT calculations to understand their interaction modes with rGOs. This study is significant because (1) it is the first time that we have been able to gain a deeper understanding of the effect of the benzene-ring number and polar functional groups on the adsorption of aromatic compounds on rGOs; (2) it is useful in assessing the adsorption of coexisting aromatic compounds on rGOs; and (3) it offers us an indication of future directions to choose and to design high-efficiency adsorbents for the simultaneous removal of aromatic compounds from wastewater. Although it is relatively expensive than other natural materials and carbon materials, rGOs present the high adsorption capacity for organic pollutants. Further experiments focused on desorption and microscopic observations may help to advance the understanding of adsorption sites and mechanisms.

Acknowledgements

This work was supported by the National Natural Science Foundation of China (21577032, 21225730, 91326202, 21207135 and 41273134), the Priority Academic Program Development of Jiangsu Higher Education Institutions, the Collaborative Innovation Center of Radiation Medicine of Jiangsu Higher Education Institutions, Deanship of Scientific Research (DSR), King Abdulaziz University (41-130-36-HiCi) and the Fundamental Research Funds for the Central Universities (JB2015001).

Notes and references

1 G. X. Zhao, L. Jiang, Y. D. He, J. X. Li, H. L. Dong, X. K. Wang and W. P. Hu, *Adv. Mater.*, 2011, **23**, 3959–3963.
2 H. Kušic, B. Rasulev, D. Leszczynska, J. Leszczynski and N. Koprivanac, *Chemosphere*, 2009, **75**, 1128–1134.
3 M. Qamar, R. B. Elsayed, K. R. Alhooshani, M. I. Ahmed and D. W. Bahnemann, *ACS Appl. Mater. Interfaces*, 2015, **7**, 1257–1269.
4 S. Ammar, M. A. Oturan, L. Labiadh, A. Guersalli, R. Abdelhedi, N. Oturan and E. Brillas, *Water Res.*, 2015, **74**, 77–87.
5 K. J. Yang, B. L. Chen and L. Z. Zhu, *Sci. Rep.*, 2015, **5**, 11641.
6 A. Bahr, A. Fischer, C. Vogt and P. Bombach, *Water Res.*, 2015, **69**, 100–109.
7 R. H. Ke, Y. P. Xu, Z. J. Wang and S. U. Khan, *Environ. Sci. Technol.*, 2006, **40**, 3906–3911.
8 S. F. Yang, M. L. Gao, Z. X. Luo and Q. Yang, *Chem. Eng. J.*, 2015, **268**, 125–134.
9 L. Y. Jiang, L. Liu, S. D. Xiao and J. M. Chen, *Chem. Eng. J.*, 2016, **284**, 609–619.
10 A. Radian and Y. Mishael, *Environ. Sci. Technol.*, 2012, **46**, 6228–6235.
11 B. Pan and B. S. Xing, *Environ. Sci. Technol.*, 2008, **42**, 9005–9013.
12 X. X. Chen and B. L. Chen, *Environ. Sci. Technol.*, 2015, **49**, 6181–6189.
13 G. J. Guan, S. Y. Zhang, S. H. Liu, Y. Q. Cai, M. Low, C. P. Teng, I. Y. Phang, Y. Cheng, K. L. Duei, B. M. Srinivasan, Y. G. Zheng, Y. W. Zhang and M. Y. Han, *J. Am. Chem. Soc.*, 2015, **137**, 6152–6155.
14 Y. B. Sun, Q. Wang, C. L. Chen, X. L. Tan and X. K. Wang, *Environ. Sci. Technol.*, 2012, **46**, 6020–6027.
15 J. Wang, Z. M. Chen and B. L. Chen, *Environ. Sci. Technol.*, 2014, **48**, 4817–4825.
16 Z. X. Jin, X. X. Wang, Y. B. Sun, Y. J. Ai and X. K. Wang, *Environ. Sci. Technol.*, 2015, **49**, 9168–9175.
17 S. Xu, Z. Y. Zhang and M. Q. Chu, *Biomaterials*, 2015, **54**, 188–200.
18 S. Liu, T. H. Zeng, M. Hofmann, E. Burcombe, J. Wei, R. Jiang, J. Kong and Y. Chen, *ACS Nano*, 2011, **5**, 6971–6980.
19 O. Akhavan and E. Ghaderi, *ACS Nano*, 2010, **4**, 5731–5736.
20 J. Zhao, Z. Y. Wang, J. C. White and B. S. Xing, *Environ. Sci. Technol.*, 2014, **48**, 9995–10009.
21 K. Yang, X. L. Wang, L. Z. Zhu and B. S. Xing, *Environ. Sci. Technol.*, 2006, **40**, 5804–5810.
22 Z. Yu and W. Huang, *Environ. Sci. Technol.*, 2005, **39**, 4878–4885.
23 M. Sander and J. J. Pignatello, *Environ. Sci. Technol.*, 2005, **39**, 1606–1615.
24 N. G. Asenjo, P. Álvarez, M. Granda, C. Blanco, R. Santamaría and R. Menéndez, *J. Hazard. Mater.*, 2011, **192**, 1525–1532.
25 C. J. Liang and Y. J. Chen, *J. Hazard. Mater.*, 2010, **182**, 544–551.
26 D. H. Lin and B. S. Xing, *Environ. Sci. Technol.*, 2008, **42**, 7254–7259.
27 S. Gotovac, H. Honda, Y. Hattori, K. Takahashi, H. Kanoh and K. Kaneko, *Nano Lett.*, 2007, **7**, 583–587.
28 S. Stankovich, D. A. Dikin, R. D. Piner, K. A. Kohlhaas, A. Kleinhammes, Y. Y. Jia, Y. Wu, S. T. Nguyen and R. S. Ruoff, *Carbon*, 2007, **45**, 1558–1565.

29 A. D. Becke, *J. Chem. Phys.*, 1993, **98**, 5648–5652.
30 A. D. Becke, *J. Chem. Phys.*, 1996, **104**, 1040–1046.
31 C. Lee, W. T. Yang and R. G. Parr, *Phys. Rev. B*, 1988, **37**, 785–789.
32 L. Goerigk and S. A. Grimme, *Phys. Chem. Chem. Phys.*, 2011, **13**, 6670–6688.
33 S. Grimme, J. Antony, S. Ehrlich and H. Krieg, *J. Chem. Phys.*, 2010, **132**, 154104.
34 S. Grimme, *J. Comput. Chem.*, 2004, **25**, 1463–1473.
35 A. Klamt and G. Schüürmann, *J. Chem. Soc., Perkin Trans.*, 1993, **2**, 799–805.
36 R. Cammi, B. Mennucci and J. Tomasi, *J. Phys. Chem. A*, 1999, **103**, 9100–9108.
37 J. Tomasi, B. Mennucci and R. Cammi, *Chem. Rev.*, 2005, **105**, 2999–3093.
38 M. J. Frisch, G. W. Trucks, H. B. Schlegel, G. E. Scuseria, M. A. Robb, J. R. Cheeseman, G. Scalmani, V. Barone, B. Mennucci, G. A. Petersson, H. Nakatsuji, M. Caricato, X. Li, H. P. Hratchian, A. F. Izmaylov, J. Bloino, G. Zheng, J. L. Sonnenberg, M. Hada, M. Ehara, K. Toyota, R. Fukuda, J. Hasegawa, M. Ishida, T. Nakajima, Y. Honda, O. Kitao, H. Nakai, T. Vreven, J. A. Montgomery, Jr., J. E. Peralta, F. Ogliaro, M. Bearpark, J. J. Heyd, E. Brothers, K. N. Kudin, V. N. Staroverov, R. Kobayashi, J. Normand, K. Raghavachari, A. Rendell, J. C. Burant, S. S. Iyengar, J. Tomasi, M. Cossi, N. Rega, J. M. Millam, M. Klene, J. E. Knox, J. B. Cross, V. Bakken, C. Adamo, J. Jaramillo, R. Gomperts, R. E. Stratmann, O. Yazyev, A. J. Austin, R. Cammi, C. Pomelli, J. Ochterski, R. L. Martin, K. Morokuma, V. G. Zakrzewski, G. A. Voth, P. Salvador, J. J. Dannenberg, S. Dapprich, A. D. Daniels, O. Farkas, J. B. Foresman, J. V. Ortiz, J. Cioslowski and D. J. Fox, *GAUSSIAN 09 (Revision A.1)*, Gaussian, Inc., Wallingford, CT, 2009.
39 L. Y. Ma, B. Yu, X. D. Qian, W. Yang, H. F. Pan, Y. Q. Shi, L. Song and Y. Hu, *Polym. Adv. Technol.*, 2014, **25**, 605–612.
40 T. N. Lambert, C. C. Luhrs, C. A. Chavez, S. Wakeland, M. T. Brumbach and T. M. Alam, *Carbon*, 2010, **48**, 4081–4089.
41 D. X. Yang, A. Velamakanni, G. Bozoklu, S. Park, M. Stoller, R. D. Piner, S. Stankovich, I. Jung, D. A. Field, C. Ventrice and R. S. Ruoff, *Carbon*, 2009, **47**, 145–152.
42 Y. B. Sun, D. D. Shao, C. L. Chen, S. B. Yang and X. K. Wang, *Environ. Sci. Technol.*, 2013, **47**, 9904–9910.
43 N. A. Kumar, H. J. Choi, Y. R. Shin, D. W. Chang, L. Dai and J. B. Baek, *ACS Nano*, 2012, **6**, 1715–1723.
44 S. J. Yu, Q. Wei, B. Du, D. Wu, H. Li, L. G. Yan, H. M. Ma and Y. Zhang, *Biosens. Bioelectron.*, 2013, **48**, 224–229.
45 I. Calizo, A. Balandin, W. Bao, F. Miao and C. Lau, *Nano Lett.*, 2007, **7**, 2645–2649.
46 H. Gao, F. Xiao, C. Ching and H. Duan, *ACS Appl. Mater. Interfaces*, 2011, **3**, 3049–3057.
47 J. Shen, Y. Hu, C. Li, C. Qin and M. Ye, *Small*, 2009, **5**, 82–85.
48 I. Langmuir, *J. Am. Chem. Soc.*, 1918, **40**, 1361–1403.
49 H. M. F. Freundlich, *J. Phys. Chem.*, 1906, **57**, 385–470.
50 R. Sips, *J. Chem. Phys.*, 1948, **16**, 490–495.
51 K. Yang, W. H. Wu, Q. F. Jing, W. Jiang and B. S. Xing, *Environ. Sci. Technol.*, 2010, **44**, 3021–3027.
52 A. Kaibara, M. Hirose and T. Nakagawa, *Chromatographia*, 1990, **29**, 551–556.
53 M. T. McDermott and R. L. McCreery, *Langmuir*, 1994, **10**, 4307–4314.
54 F. A. Carey, *Organic Chemistry*, 6th edn, McGraw-Hill, New York, 2005.
55 W. Chen, L. Duan, L. L. Wang and D. Q. Zhu, *Environ. Sci. Technol.*, 2008, **42**, 6862–6868.
56 M. Y. Zou, J. D. Zhang, J. W. Chen and X. H. Li, *Environ. Sci. Technol.*, 2012, **46**, 8887–8894.
57 R. Hao, W. Qian, L. H. Zhang and Y. L. Hou, *Chem. Commun.*, 2008, 6576–6578.
58 C. Hu, S. Sedghi, A. Silvestre-Albero, G. G. Andersson, A. Sharma, P. Pendleton, F. Rodríguez-Reinoso, K. Kaneko and M. J. Biggs, *Carbon*, 2015, **85**, 147–158.
59 X. L. Wang, S. Tao and B. S. Xing, *Environ. Sci. Technol.*, 2009, **43**, 6214–6219.
60 D. Cortes-Arriagada, L. Sanhueza and M. Santander-Nelli, *J. Mol. Model.*, 2013, **19**, 3569–3580.

